**TABLE 1 Comparison of Mixer in this Work with the One in Refs. [5], [7], and [8]**

| | Device ($\mu$m) | 3 dB Bandwidth (GHz) and IF Frequency | Gain (dB) | LO to RF Isolation (dB) | P1dB (dBm) | Power (mW) |
|---|---|---|---|---|---|---|
| Ref. [5] | 0.18 | 1 (LNA+Mixer) IF Frequency (5 GHz) | 13 | – | -23 (LNA+Mixer) | 40.5 |
| Ref. [7] | 0.18 | 1.4 IF Frequency (100 MHz) | 1.2 | Less than -30 | -3 | 45 |
| Ref. [8] | 0.13 | 1.4 IF Frequency (2.7 GHz) | 1 | Less than -40 | -2 (IIP3) | 6.9 |
| This work | 0.18 | 1.9 IF Frequency (100 MHz) | 3.4 | Less than -40 | -4 | 36 |

### 3. MEASUREMENT RESULTS

The designed mixer was measured by bare chip probing and coaxial cable connection. The RF and LO ports are contacted with GSG probes of 100 $\mu$m pitch. The IF port is connected to a SMA connector through bonding wires and FR-4 substrate. The measured conversion gain of mixer is between $-1$ and 3.4 dB at the RF frequency from 23 to 25.1 GHz and the fixed LO frequency of 24.1 GHz with LO power of 0 dBm as shown in Figure 3. The 3-dB bandwidth obtains 1.9 GHz at RF signal from 23.1 to 25 GHz. Figure 4 shows the measured return loss for RF and LO ports. The RF and LO return losses show less than $-15$ dB and $-7$ dB at the frequency of 20–26.5 GHz, respectively. These wideband characteristics are similar to the balun. The measured isolation performance is shown in Figure 5. The RF to LO and LO to RF isolations achieve less than $-40$ dB at 20–26.5 GHz. Figure 6 shows the input 1 dB compression point (input P1dB), which is $-4$ dBm. The comparison of the designed mixer with the one in [5], [7], and [8] is shown in Table 1.

### 4. CONCLUSION

The K-band double balanced mixer based on Gilbert-cell type in 0.18 $\mu$m CMOS technology is presented. The proposed balun circuits are used for the matching network at the RF and LO ports of the mixer to increase bandwidth. The mixer achieves a 3-dB bandwidth of 1.9 GHz while dissipating the power of 36 mW at 1.8 V supply. This mixer may be applied to the short range automotive radar with a high range resolution of less than 10 cm.

### ACKNOWLEDGMENT

This work was supported by the Center for Distributed Sensor Network at Gwangju Institute of Science and Technology (GIST) and the BK21 program in the Republic of Korea.

### REFERENCES

1. H. Shigematsu, T. Hirose, F. Brewer, and M. Rodwell, Millimeter-wave CMOS circuit design, IEEE Trans Microw Theory Tech 53 (2005), 472–477.
2. K.W. Yu, Y.L. Lu, D.C. Chang, V. Liang, and M.F. Chang, K-band low noise amplifiers using 0.18 $\mu$m CMOS technology, IEEE Microw Wireless Compon Lett 14 (2004), 106–168.
3. H.H. Hsieh and L.H. Lu, A low-phase-noise K-band CMOS VCO, IEEE Microw Wireless Compon Lett 16 (2006), 552–554.
4. J.H. Tasi, P.S. Wu, and C.S. Lin, A 25-75 GHz broadband Gilbert-cell mixer using 90-nm CMOS technology, IEEE Microw Wireless Compon Lett 17 (2007), 247–249.
5. X. Guan and A. Hajimiri, A 24-GHz CMOS front-end, IEEE J Solid State Circ 39 (2004), 368–373.
6. M.D. Tasi and H. Wang, A 0.3-25 GHz ultra-wideband mixer using commercial 0.18-$\mu$m CMOS technology, IEEE Microw Wireless Compon Lett 14 (2004), 522–524.
7. H.Y. Yu, S.S. Choi, S.H. Kim, and Y.H. Kim, K-band single balanced mixer for ultra-wideband radar in 0.18 $\mu$m CMOS technology, Microw Opt Tech Lett 49 (2007), 2697–2700.
8. A. Verma, Li. Gao, K.O. Kenneth, and J. Lin, A K-band down-conversion mixer with 1.4 GHz bandwidth in 0.13 $\mu$m CMOS technology, IEEE Microw Wireless Compon Lett 15 (2005), 493–495.
9. H.Y. Yu, S.S. Choi, S.H. Kim, and Y.H. Kim, K-band balun with slot pattern ground for wide operation using 0.18 $\mu$m CMOS technology, Electron Lett 43 (2007), 293–295.



# A SIMPLE SMART COMPOSITE USING FIBER BRAGG GRATING SENSORS FOR STRAIN AND TEMPERATURE DISCRIMINATION

**O. Frazão,[1] R. Oliveira,[2] and I. Dias[1]**
[1] INESC Porto - Unidade de Optoelectrónica e Sistemas Electrónicos, Rua do Campo Alegre, 687, 4169–007 Porto, Portugal; Corresponding author: ofrazao@inescporto.pt
[2] INEGI - Instituto de Engenharia Mecânica e Gestão Industrial, Rua do Barroco, 174, 4465–591 Leça do Balio, Portugal

*Received 22 May 2008*

**ABSTRACT:** *A smart laminated composite with a simple geometry was produced with embedded fiber Bragg grating sensors. The smart structure is composed of two Bragg gratings located in regions of different thicknesses of the laminated composite. Although one of the Bragg gratings is embedded between two layers, the other is embedded in four layers. When the strain is applied to the smart composite, different response is obtained. Because of this characteristic it is possible to discriminate strain and temperature using a traditional matrix method. To reduce the inherent error, an artificial neural network approach is proposed that will improve the strain and temperature measurement discrimination when using this new configuration. These instrumented carbon fiber laminates can be used for monitoring of reinforcement and protection of structures.* © 2008 Wiley Periodicals, Inc. Microwave Opt Technol Lett 51: 235–239, 2009; Published online in Wiley InterScience (www.interscience.wiley.com). DOI 10.1002/mop.23990

**Key words:** *fiber Bragg grating sensors; artificial neural network*

### 1. INTRODUCTION

According to Culshaw [1], a smart structure can be defined as one that monitors itself and/or its environment in order to respond to changes in its condition. Fiber Bragg grating sensors (FBG) can be very useful in applications where layered materials, such as composites, are involved. Because of the fact that fiber optic sensors are small, multiplexable, electrically isolated and immune to electromagnetic fields, they can give engineers the possibility to incorporate a fiber optic nervous systems into their composite material designs. These sensors allow measurement of parameters such as load/strain, vibration, temperature, detection of cracks, and delamination phenomena [1]. When FBGs are applied to the measurement of strain their cross-sensitivity to temperature is an issue

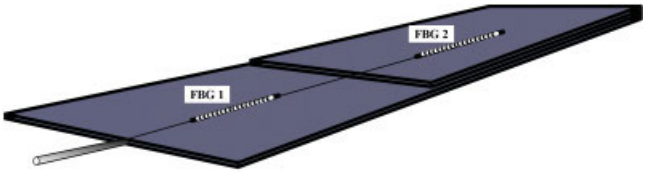


**Figure 1** Geometry of the sensing head. [Color figure can be viewed in the online issue, which is available at www.interscience.wiley.com]

that needs to be addressed. One approach to solve this issue it is to design sensing heads insensitive to temperature. Another one is the conception of structures with sufficient degrees of freedom to permit the simultaneous discrimination of these two parameters. Many researchers have worked out this path and a significant number of configurations exhibiting this discrimination functionality have been proposed. In the FBG technology, fibers with different diameters [2], are examples of workable solutions for strain/temperature discrimination. Other authors have followed this path and new configurations based on chirped taper FBG [3] or twisted configuration [4]. These three examples present different sensitivities to strain but similar sensitivity to temperature. Nevertheless all these configurations are fragile due to their geometry. To embed the Bragg grating in composite materials eliminates this fragility.

Several authors have already proposed some solutions using optical fibers embedded in a laminated composite. Zhang et al. [5] presented a multimode optical fiber that can monitor the viscosity of resin during the composite processing. A detection of impact damage in stiffened composite panels, using embedded small-diameter optical fibers was also proposed by Tsutsui et al. [6]. Zhao and Ansari [7] proposed a distributed fiber optic sensor system for strain measurement over the interfacial zones of carbon fibers bonded reinforced concrete. On the other hand, Tanaka et al. [8] proposed for the first time a temperature compensated hybrid composite, for strain measurement using Bragg gratings embedded in a laminated composite. In this case, the smart composite consisted of carbon fiber reinforced plastic (CFRP) and glass fiber reinforced plastic (GFRP) connected in series.

In this work, the authors present an alternative solution of fiber Bragg grating embedded in laminated composite with different layers. Because of different response to strain, this configuration can solve the problem of cross-sensitivity to temperature. An artificial neural approach was used to reduce the errors obtained by the matrix method.

## 2. EXPERIMENTAL RESULTS

The system used for monitoring the smart laminated composite included an optical spectrum analyzer (ANDO AQ 6330), an erbium broadband optical source (PHOTONETICS), a 3 dB coupler, and a computer data acquisition system. Two fiber Bragg gratings (1530 and 1550 nm) were embedded between layers of pre-impregnated carbon fiber/epoxy resin (The laminates is cross-ply $\%_{(s)}$ with dimensions of $150 \times 70 \times 0.33$ mm$^3$) to produce a smart laminated composite (see Fig. 1). One of the Bragg gratings is embedded between two layers and the other Bragg grating is embedded between four layers. The smart composite with the Bragg gratings was cured inside an autoclave at 100°C during 1 h with a pressure of $0.8 \times 10^5$ Pa.

After the cure, the smart composite was characterized concerning strain (using a test machine INSTRON (mod. 4208)) and temperature. This characterization consisted in temperature measurements holding strain constant ($\varepsilon = 0$) and strain measurements induced by strain holding constant temperature ($T = 20$°C). Figures 2 and 3 shows the response of the two FBGs to temperature variation under constant strain and strain variation at constant temperature, respectively.

Figure 2 presents different strain sensitivities of smart composite when is subjected to strain. The difference is due to the Bragg gratings are embedded in different number layers. Relatively to the temperature, a nonlinear response is obtained. This response is due to the fact that the epoxy resin in the pre-impregnated of CFRP has a nonlinear response when it is subjected to temperature. The small difference between the responses of the Bragg gratings is due to

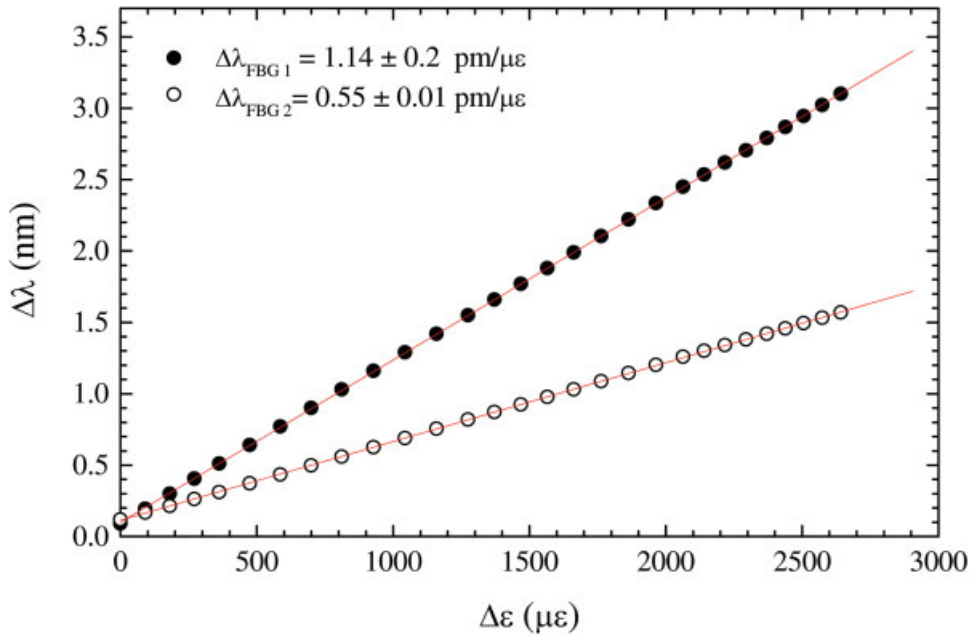


**Figure 2** Response of the sensing head to strain. [Color figure can be viewed in the online issue, which is available at www.interscience.wiley.com]

the dependence of the wavelength of the FBGs with the temperature.

These results permit to write a well-conditioned system of two equations for $\Delta T$ and $\Delta\varepsilon$, given in a matrix form as

$$\begin{bmatrix}\Delta\lambda_{\mathrm{FBG1}}\\ \Delta\lambda_{\mathrm{FBG2}}\end{bmatrix}=\begin{bmatrix}b_1 & 0\\ b_2 & 0\end{bmatrix}+\begin{bmatrix}\kappa_{T1} & \kappa_{\varepsilon1}\\ \kappa_{T2} & \kappa_{\varepsilon2}\end{bmatrix}\begin{bmatrix}\Delta T\\ \Delta\varepsilon\end{bmatrix}+\begin{bmatrix}a_1 & 0\\ a_2 & 0\end{bmatrix}\begin{bmatrix}\Delta T^2\\ \Delta\varepsilon^2\end{bmatrix} \quad (1)$$

and the solution obtained for $\Delta T$ and $\Delta\varepsilon$ is

$$\Delta T=\frac{-\left(\kappa_{T2}-\kappa_{T1}\frac{\kappa_{\varepsilon2}}{\kappa_{\varepsilon1}}\right)\pm\sqrt{\left(\kappa_{T2}-\kappa_{T1}\frac{\kappa_{\varepsilon2}}{\kappa_{\varepsilon1}}\right)^2-4\left(a_{2_1}-a_1\frac{\kappa_{\varepsilon2}}{\kappa_{\varepsilon1}}\right)\left(\frac{\kappa_{\varepsilon2}}{\kappa_{\varepsilon1}}(\Delta\lambda_{FBG1}-b_1)-(\Delta\lambda_{FBG2}-b_2)\right)}}{2\left(a_2-a_1\frac{\kappa_{\varepsilon2}}{\kappa_{\varepsilon1}}\right)} \quad (2)$$

$$\Delta\varepsilon=\frac{1}{\kappa_{\varepsilon1}}[\Delta\lambda_{FBG1}-\kappa_{T1}\Delta T-a_1\Delta T^2]$$

Replacing all the coefficient parameters, we obtained the following results:

$$\begin{bmatrix}\Delta\lambda_{\mathrm{FBG1}}\\ \Delta\lambda_{\mathrm{FBG2}}\end{bmatrix}=\begin{bmatrix}4.63 & 0\\ 3.34 & 0\end{bmatrix}+\begin{bmatrix}1.74 & 1.14\\ 1.59 & 0.55\end{bmatrix}\begin{bmatrix}\Delta T\\ \Delta\varepsilon\end{bmatrix}+\begin{bmatrix}0.14 & 0\\ 0.13 & 0\end{bmatrix}\times\begin{bmatrix}\Delta T^2\\ \Delta\varepsilon^2\end{bmatrix} \quad (3)$$

and the solution is

$$\Delta T=\frac{-0.755\pm\sqrt{+0.24\Delta\lambda_{FBG2}-0.11\Delta\lambda_{FBG1}-0.31}}{0.12}$$

$$\Delta\varepsilon=0.87\Delta\lambda_{FBG1}-1.51\Delta T-4.03\Delta T^2 \quad (4)$$

The system performance was evaluated when the sensing head was simultaneously subjected to strain and temperature changes over strain and temperature ranges of 2700 $\mu\varepsilon$ and 45°C, respectively. The results are shown in Figure 4. The rms deviations were found to be ±1.47°C and ±5.7 $\mu\varepsilon$ for temperature and strain measurements, respectively.

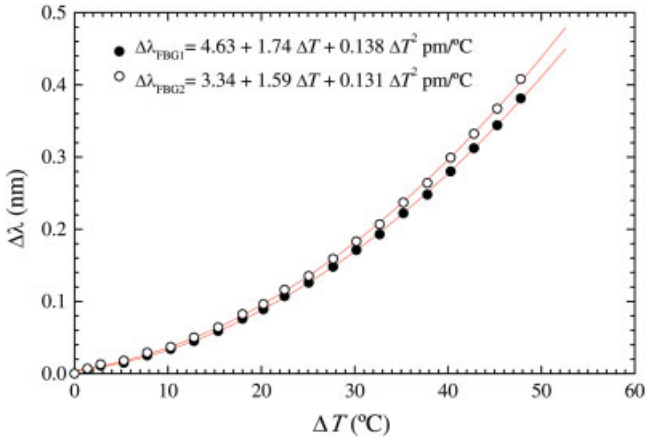


**Figure 3** Response of the sensing head to temperature. [Color figure can be viewed in the online issue, which is available at www.interscience.wiley.com]

## 3. AN ARTIFICIAL NEURAL NETWORK APPROACH

An artificial neural network (ANN) approach is proposed to improve the strain and temperature measurements cross-sensitivity. ANN has been applied to temperature and strain measurements in the case of large cross-sensitivity sensors, whose matrix inversion causes significant errors due to the nonlinear evolution of the matrix coefficients as function of $\Delta T$ and $\Delta\varepsilon$ [9].

To avoid the matrix inversion, an ANN was trained to perform a nonlinear input–output mapping. The variations $\Delta\lambda_1$ and $\Delta\lambda_2$ were given as inputs to the ANN which provides values of $\Delta T$ and $\Delta\varepsilon$ as outputs.

An ANN is an interconnected group of simple processing units (neurons) that uses a mathematical or computational model for information processing based on a connectionist approach to computation (see Fig. 5). Despite the simplicity of each processing unit, the use of many neurons guarantees the execution of multiple tasks.

The links between neurons are characterized by weights, $w_{ki}$, which modulate the effect of the associated input, $x_i$, to a neuron, $k$. A pondered sum of the weighted input is then performed. The neuron transmits an activity level transduced by a function of activation, $\varphi$.

ANN is an adaptive model that can learn from the data and generalize it. It extracts the essential characteristics from the numerical data, offering a convenient way to create an implicit model.

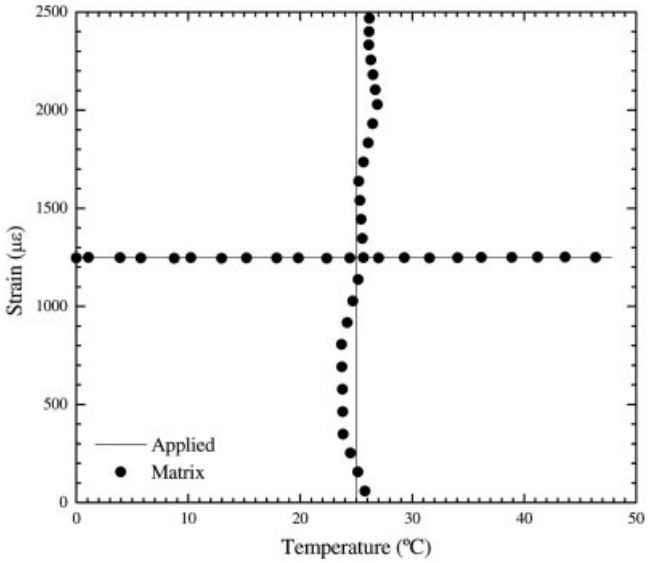


**Figure 4** Sensor output as determined by Eq. (4) for applied strain at constant temperature and temperature variation at constant strain

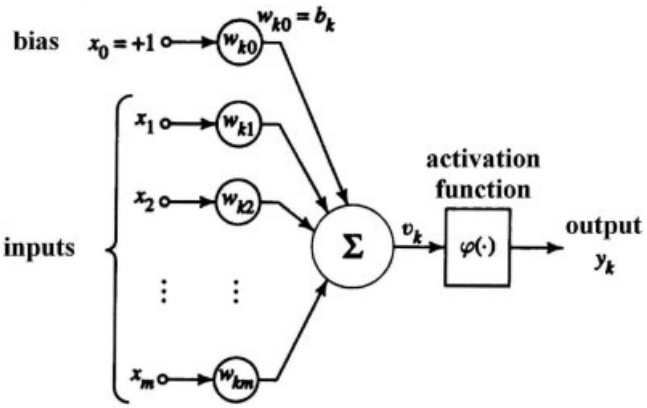


**Figure 5** Model of a neuron

The chosen network was a multilayer perceptron (MLP) trained in supervised learning with the *Levenberg-Marquardt* algorithm. The MLP is based on an input, a hidden and an output layers interconnected in a feed-forward way [10, 11]. Each neuron has directed connections to all the neurons of the subsequent layer (see Fig. 6). The neurons activation function in the hidden layer is the nonlinear sigmoid function whereas in the output layer it is the linear function. The network output is thus a linear combination of the outputs of the hidden neurons with $\alpha_{jk}$ defining the synaptic weights of output layer.

The MLP outputs are compared with the pretended predefined target using an error-function. This error is then fed back through the network. Using this information, the algorithm adjusts the weights of each connection in order to reduce the error value. The process is repeated until the network converges to some state where the error is small. In this case the network has learned a certain target function.

The universal approximation theorem for ANN states that every continuous function that maps intervals of real numbers to some output interval of real numbers can be approximated arbitrarily closely by a MLP with just one hidden layer [11]. $\Delta T$ and $\Delta\varepsilon$ can thus be approximated as follows

$$\begin{cases} \left| \Delta T - \sum_{k=1}^{m} \alpha_{1k} \varphi(w_{k1}\lambda_{\text{conv}} + w_{k2}\lambda_{\text{sat}} + b_k) \right| < \in_1 \\ \left| \Delta\varepsilon - \sum_{k=1}^{m} \alpha_{2k} \varphi(w_{k1}\lambda_{\text{conv}} + w_{k2}\lambda_{\text{sat}} + b_k) \right| < \in_2 \end{cases} \quad (6)$$

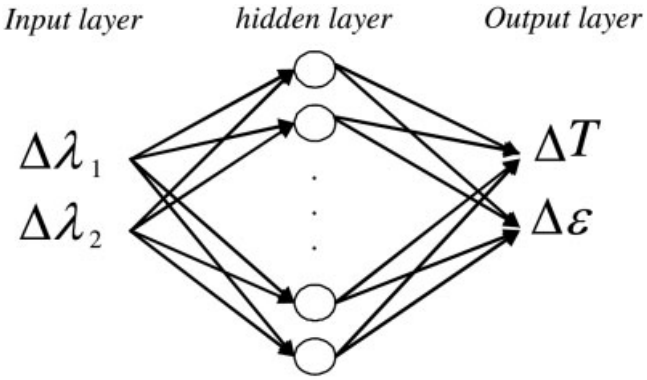


**Figure 6** Architectural graph of a MLP with one hidden layer

where $\varphi$ is the sigmoid function, $b_k$ the bias, $\epsilon_j$ the approximation errors and $m$ the number of neurons in the hidden layer.

The hidden layer of the chosen MLP is constituted of 10 neurons. Classical back-propagation training algorithm is based on the gradient descent method. This method is often too slow for practical problems. The *Levenberg-Marquardt* back-propagation algorithm is then used here instead of MLP training because of having a faster convergence [11]. The performance of the trained ANN is measured using the mean square error.

Data analysis was performed using MATLAB® Neural Network Toolbox [12]. The network inputs consist of pairs of ($\Delta\lambda_1$, $\Delta\lambda_2$). During the training the MLP is adjusted to relate these input pairs to their respective target pair ($\Delta T$, $\Delta\varepsilon$).

The training efficiency highly depends on the data used for training. This data must be representative of the underlying model. Training data consisted of 3400 pairs of ($\Delta T$, $\Delta\varepsilon$) values generated, within a range of 0–2700 $\mu\varepsilon$ and 0–45°C, by interpolation of the experimental values. The respective pairs of ($\Delta\lambda_1$, $\Delta\lambda_2$) were obtained applying the Eq. (3). To improve the training efficiency the data was pre-processed. Inputs and targets were normalized to have zero mean and unity standard deviation to guarantee that they have the same relevance.

The generalization ability of the trained MLP network was then verified with a set of another 100 pairs of simulated data.

The performance of the two techniques (matrix method and ANN) was evaluated when the sensing head undertook strain variations in a range of 2700 $\mu\varepsilon$ at a fixed temperature ($\Delta T$ = 20°C) and the other way around, i.e., temperature variations in a range of 50°C for a specific applied strain ($\Delta\varepsilon$ = 1250 $\mu\varepsilon$).

The results using both methods are presented in Figure 7. For the matrix the maximum errors were ±1.47°C and ±5.7 $\mu\varepsilon$ for temperatures and strain, respectively.

For the ANN method a satisfactorily generalization of data was achieved. The resulting maximum errors for the ANN method were found to be ±0.2°C and ±1.9 $\mu\varepsilon$ for temperature and strain measurements, respectively.

## 4. CONCLUSIONS

In this work, the authors presented an alternative smart composite based on Bragg grating structure embedded between of layers of

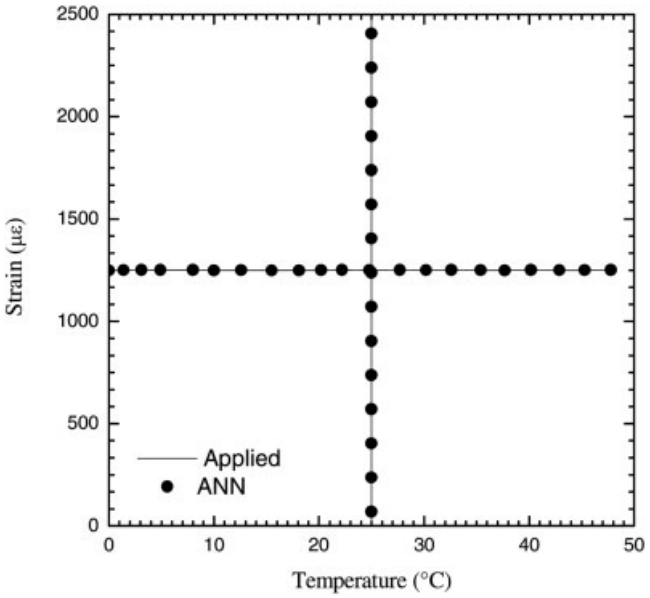


**Figure 7** Sensor output as determined by ANN

pre-impregnated carbon fiber/epoxy resin. Because of its geometry, the smart composite can simultaneously discriminate the strain and the temperature. To reduce the errors of the matrix methods, an ANN approach is proposed to improve the strain and temperature measurements cross-sensitivity. The Figures 4 and 7 show the difference between the temperature fluctuation using the matrix method and the ANN. The fluctuation of the error is due to the non linear response of the epoxy resin subjected to temperature variations. The use of the ANN in this case, reduced seven times the temperature error and three times the strain error. We can conclude that the ANN is a good approach modeling the response of a nonlinear sensing head when subjected to the action of physical parameters. In fact this solution can be applied in several applications, namely, where this composite is used in great structure of engineering.

## REFERENCES


1. B. Culshaw. Smart structures and Materials, Artech House Publishers, Norwood, MA, 1996.
2. S.W. James, M.L. Dockney, and F.P. Tatam Simultaneous independent temperature and strain measurement using in-fibre Bragg grating sensors, Electron Lett 32 (1996), 1133–1134.
3. O. Frazão, M. Melo, P.V.S. Marques, and J.L. Santos, Chirped Bragg grating fabricated in fused fibre taper for strain-temperature discrimination, Meas Sci Technol 16 (2005), 984–988.
4. O. Frazão, L.A. Ferreira, F.M. Araújo, and J.L. Santos, Simultaneous measurement of strain and temperature using Bragg gratings in a twisted configuration, J Opt A: Pure Appl Opt 7 (2005), 427–430.
5. B. Zhang, Z. Wu, D. Wang, and S. Du, Investigation of multifunctional fiber optic sensor in smart composite, Opt Eng 40 (2001), 612–617.
6. H. Tsutsui, A. Kawamata, T. Sanda, and N. Takeda, Detection of impact damage of stiffened composite panels using embedded small-diameter optical fibers, Smart Mater Struct 13 (2004), 1284–1290.
7. Y. Zhao and F. Ansari, Embedded fiber optic sensor for characterization of interface strains in FRP composite, Sens Actuator A 100 (2002), 247–251.
8. N. Tanaka, Y. Okabe, and N. Takeda, Temperature-compensated strain measurement using fiber Bragg grating sensors embedded in composite laminates, Smart Mater Struct 12 (2003), 940–946.
9. C.C. Chan, W. Jin, A.B. Rad, and M.S. Demokan, Simultaneous measurement of temperature and strain: an artificial neural network approach; Photon Technol Lett IEEE 10 (1998), 854–856.
10. S. Haykin, Neural Networks: A comprehensive foundation, Chapter 4: Multilayer Perceptrons, Prentice Hall, Upper Saddle River, NJ, 1999, pp. 156.
11. C. Bishop, Neural networks for pattern recognition, Chapter 4: The Multi-layer Perceptron, Oxford University Press, Oxford, 1995, p. 116.
12. H. Demuth and M. Beale, Neural Network Toolbox User′s Guide, Version 4.




# COMPACT BROADBAND PLANAR ANTENNA FOR DVB-H APPLICATIONS

**Ma Hanqing and Qing-Xin Chu**
School of Electronic and Information Engineering, South China University of Technology, Guangzhou, Guangdong, China;
Corresponding author: vswr@163.com

*Received 28 May 2008*

**ABSTRACT:** *A novel compact broadband planar antenna for digital television signal reception is presented. The antenna consists of a folded radiating patch and a parasitic arm, which are easily printed on an FR4 substrate. The antenna occupies an area of only 70 × 42 mm², while it covers a bandwidth (3:1 VSWR) of 360 MHz (460–820 MHz). Moreover, it has dipole-like radiation patterns within its operation band with gain values larger than 0 dBi.* © 2008 Wiley Periodicals, Inc. Microwave Opt Technol Lett 51: 239–242, 2009; Published online in Wiley InterScience (www.interscience.wiley.com). DOI 10.1002/mop.24024

**Key words:** *antenna; planar antenna; DTV; broadband antenna; compact antenna*

## 1. INTRODUCTION

Digital television (DTV) has already been standard for delivering broadcast television to mobile terminals such as mobile phone, PMP, PDA, etc. Thus the antenna solution for small handheld terminals has taken a growing interest. One of the major challenges is the design of terminal antennas that are compact in size but have wide impedance matched band and high radiation efficiency. Many

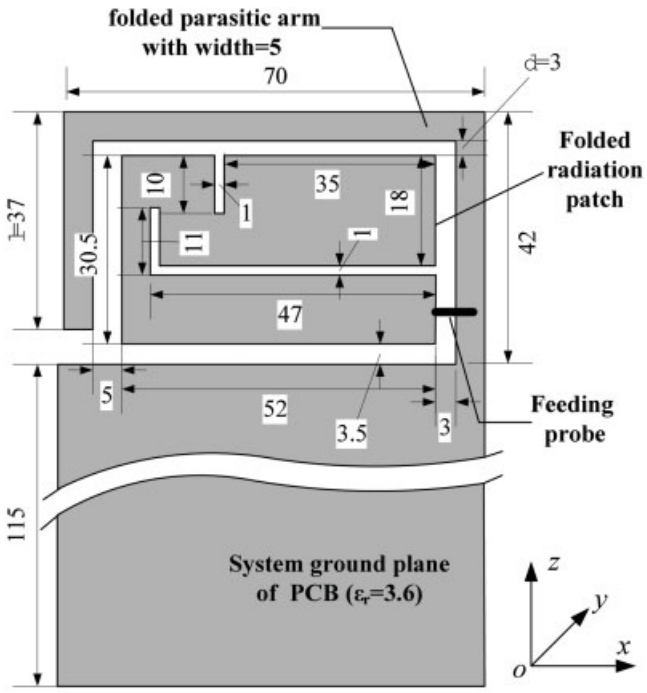


(a)

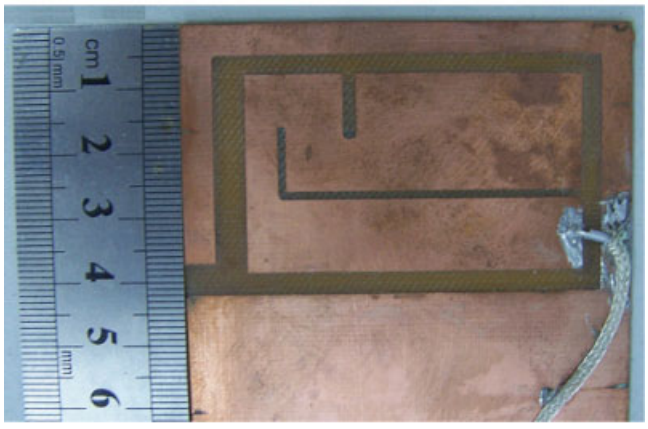

(b)

**Figure 1** Antenna geometry and photograph. (a) Geometry of the antenna, (unit: mm). (b) Photograph of the antenna. [Color figure can be viewed in the online issue, which is available at www.interscience.wiley.com]